Addition *in the dark* of PMe_3 to a benzene solution of $[Mn(CO)_3depe]_n$ and $Mn_2(CO)_{10}$ (1:2) results in the gradual disappearance of the $Mn_2(CO)_{10}$ and $[Mn(CO)_3depe]_2$ and the appearance of $Mn(CO)_5^-$ and $Mn(CO)_3L_3^+$. The anionic product was identified by infrared spectroscopy[3] (ν(C≡O) = 1906 (sh), 1889 (s), 1865 (s), 1842 (sh) cm^{-1} (in C_6H_6); ν(C≡O) = 1900 (s), 1861 (s) cm^{-1} (in CH_2Cl_2)). By comparison to literature infrared spectra, the cationic product (ν(C≡O) = 2016 (m), 1935 (s) cm^{-1} (in C_6H_6); ν(C≡O) = 2021 (m), 1946 (s) cm^{-1} (in CH_2Cl_2)) could only be identified as *fac*-$Mn(CO)_3L_3^+$ (L = phosphine). (For example, ν(C≡O) bands for $[Mn(CO)_3(PEt_3)_3][ClO_4]$ are 2021 (s) and 1943 (s) cm^{-1}, in CH_2Cl_2.[9]) Presumably, the cation can be formulated as *fac*-$Mn(CO)_3(depe)(PMe_3)^+$. Scheme IV accounts for these results. Essentially we are proposing that the 17-electron $Mn(CO)_3depe$ complex reacts with PMe_3 to form the 19-electron $Mn(CO)_3(depe)PMe_3$ complex, which then reduces $Mn_2(CO)_{10}$ as in the disproportionation mechanism (Scheme I). Note that the three phosphorus ligands of the 19-electron $Mn(CO)_3(depe)PMe_3$ species have a smaller cone angle sum (θ_{total} = 348° = 230° (bidentate depe) + 118° (PMe_3)) than do those of either $Mn(CO)_3(PMe_3)_3$ (θ_{total} = 354°) or $Mn(CO)_3$(depe-*P*,*P*′)(depe-*P*) ($\theta_{total} \approx 362° = 230°$ (bidentate depe) + ~132° (monodentate depe, assumed to be approximately equal to $\theta(PEt_3)$)).[15] Evidently, the smaller total size of the depe and PMe_3 ligands permits the formation of the mixed-phosphine 19-electron species and disproportionation occurs.

Scheme IV

$$[Mn(CO)_3depe]_2 \rightleftharpoons 2Mn(CO)_3depe \quad (19)$$

$$Mn(CO)_3depe + PMe_3 \rightleftharpoons Mn(CO)_3(depe)PMe_3 \quad (20)$$

$$Mn(CO)_3(depe)PMe_3 + Mn_2(CO)_{10} \rightarrow Mn(CO)_3(depe)(PMe_3)^+ + Mn_2(CO)_{10}^- \quad (21)$$

$$Mn_2(CO)_{10}^- \rightarrow Mn(CO)_5^- + Mn(CO)_5 \quad (22)$$

Acknowledgment is made to donors of the Petroleum Research Fund, administered by the American Chemical Society, and to the National Science Foundation for the support of this work. Derek Santiago, Frank McGorty, and Luanne Rolly are thanked for their experimental assistance.

Registry No. py, 110-86-1; dien, 111-40-0; en, 107-15-3; dmpe, 23936-60-9; depe, 6411-21-8; dppe, 1663-45-2; triphos, 23582-02-7; THF, 109-99-9; tetraphos, 23582-04-9; $Mn_2(CO)_{10}$, 10170-69-1; $Mn(CO)_5^-$, 14971-26-7; NEt_3, 121-44-8; NH_2Cy, 108-91-8; CH_3CN, 75-05-8; acetone, 67-64-1.

(21) Brown and co-workers have found that long-lived radicals of the type $M(CO)_3L_2$ (M = Mn, Re; L = tertiary phosphine or phosphite) can be generated by irradiation of the corresponding $M_2(CO)_{10}$ dimers in the presence of excess L.[22] The tendency of these species not to undergo dimerization is primarily a result of their great steric bulk. The generation of $Mn(CO)_3L_2$ requires prolonged irradiation and frequent removal of the CO generated in order to drive the reaction to completion. As we report elsewhere,[4] complexes of the type $Mn(CO)_3L_3$ can be conveniently and quantum efficiently generated by irradiation of 1:2 solutions of $Mn_2(CO)_{10}$ and bidentate phosphines such as depe. Because depe is less sterically bulky than the phosphines used by Brown, a greater tendency to dimerization is observed.

(22) (a) Kidd, D. R.; Cheng, C. P.; Brown, T. L. *J. Am. Chem. Soc.* **1978**, *100*, 4103–4107. (b) McCullen, S. B.; Brown, T. D. *J. Am. Chem. Soc.* **1982**, *104*, 7496–7500. (c) Walker, H. W.; Rattinger, G. B.; Belford, R. L.; Brown, T. L. *Organometallics* **1983**, *2*, 775–776.

Contribution from the Department of Chemistry, Harvard University, Cambridge, Massachusetts 02138

Solution Chemistry of Ethane-1,2-dithiolate Complexes: Equilibria and Electron-Transfer Reactions

R. N. Mukherjee, Ch. Pulla Rao, and R. H. Holm*

Received January 16, 1986

The first-transition-series complexes of ethane-1,2-dithiolate (edt) constitute the structurally most diverse set of homoleptic complexes yet characterized. Following prior reports of synthesis and solid-state structures, the present investigation provides definition of the structures and redox reactions of $[Ti(edt)_3]^{2-}$, $[V_2(edt)_4]^{2-}$, $[Cr(edt)_2]^{2-}$, $[Co(edt)_2]^{2-}$, $[Co(edt)_2]^-$, $[Fe_2(edt)_4]^{2-}$, and $[Mn_2(edt)_4]^{2-}$ in aprotic solvents. All species possess characteristic absorption spectra dominated by LMCT features, and all are redox-active. The results of coulometry and cyclic voltammetry are presented. $[Ti(edt)_3]^{2-}$ ($E_{p,c}$ = −2.09 V vs. SCE (MeCN)) and $[Cr(edt)_2]^{2-}$ ($E_{p,c}$ = −1.00 V (DMF)) are irreversibly reduced and oxidized, respectively; all other species exhibit chemically reversible electron-transfer reactions ($i_{p,c}/i_{p,a} \cong 1$). $[Cr(edt)_2]^{2-}$ (4.95 μ_B) retains its planar structure in solution. Planar $[Co(edt)_2]^-$ and tetrahedral $[Co(edt)_2]^{2-}$ are reversibly interconverted at $E_{1/2}$ = −1.16 V (MeCN). These species were generated separately by controlled-potential electrolysis of acetonitrile solutions prepared from $(Me_4N)_3[Co_2(edt)_4]$, which contains a 1:1 ratio of these species. The weak paramagnetism of $[V_2(edt)_4]^{2-}$ (0.9 μ_B, MeCN) indicates retention of its unusual tetrabridged structure in solution. Oxidation at $E_{1/2}$ = −0.61 V (MeCN) gives the somewhat unstable complex $[V_2(edt)_4]^-$, which was not isolated. The other two $[M_2(edt)_4]^{2-}$ complexes (M = Fe(III), Mn(III)) have lateral doubly bridged dimeric structures in the solid state. In solution they exhibit solvent- and concentration-dependent magnetic behavior consistent with the equilibrium $[M_2(edt)_4]^{2-} \rightleftharpoons 2[M(edt)_2(solv)_2]^-$. The mole fraction of monomer is higher in Me_2SO than in MeCN. $[Fe_2(edt)_4]^{2-}$ is not detectably dissociated in acetonitrile. These species are reversibly reduced to tetrahedral $[M(edt)_2]^{2-}$ at $E_{1/2}$ = −1.13 V (Fe) and −0.94 V (Mn) in acetonitrile. An ECE-type mechanism is established by cyclic voltammetry and chronoamperometry for the reduction of $[Fe_2(edt)_4]^{2-}$ in acetonitrile. Apparent lability to dissociation prevented a similar determination for the $[Mn_2(edt)_4]^{2-}$ system. The electrochemistry of acetonitrile and Me_2SO solutions prepared from $[Mn_2(edt)_4]^{2-}$ showed a significant dependence on electrode surface. As manifested in large peak-to-peak separations (ΔE_p) in cyclic voltammetry, the heterogeneous electron-transfer rate constant at a Pt electrode is ~10^3 smaller than those at a glassy-carbon or basal pyrolytic graphite electrode. Solutions of the Fe(III) and Mn(III) dimers in acetonitrile solutions exhibited adsorption phenomena at a glassy-carbon electrode that had been initialized near 0 V before potential sweep. This treatment caused oxidation of the complexes and filming of the electrode, and a cathodic shift of the reduction potential of the adsorbed Mn(III) species compared to that of the diffusion-controlled process. These observations provide a rationalization of extremely large ΔE_p values (0.5–1.1 V) previously reported. Any contributions from structural changes to these values is overwhelmed by other effects. Indeed, the reaction $[Co(edt)_2]^- + e^- \rightleftharpoons [Co(edt)_2]^{2-}$ is a reversible charge transfer under conditions where the Mn systems exhibit $\Delta E_p \geq 120$ mV.

Introduction

A substantial portion of our recent work aimed at a development of the chemistry of metal thiolates, a subject pertinent to metal coordination units in a variety of proteins and enzymes containing native and nonnative metal ions, has involved complexes of ethane-1,2-dithiolate (edt).[1-4] Some 19 structural determinations of edt complexes of the first transition series,[1-9] including con-

(1) Costa, T.; Dorfman, J. R.; Hagen, K. S.; Holm, R. H. *Inorg. Chem.* **1983**, *22*, 4091.

0020-1669/86/1325-2979$01.50/0

tributions by others,[5-9] with several of these being independent investigations of compounds containing the same anion, have revealed the following stereochemical pattern: $[M(edt)_2]^{2-}$, planar (M = Cr(II), Co(III)), tetrahedral (M = Mn(II), Co(II), Zn(II), Cd(II)); $[VX(edt)_2]^{2-}$, pyramidal (X = O, S); $[Ti(edt)_3]^{2-}$, trigonal octahedral; $[M_2(edt)_4]^{2-}$, tetrabridged six-coordinate nonoctahedral (M = V(III)), doubly bridged five-coordinate (M = Mn(III), Fe(III)); $[Ni_2(edt)_3]^{2-}$, doubly bridged planar; $[Cu_3(edt)_3]^{3-}$, nonplanar Cu_3S_3 ring. The set encompasses five stoichiometric and seven stereochemical types and includes, inter alia, two types of bridging modes for $[M_2(edt)_4]^{2-}$ complexes, one of which is the first example of a quadruple bridge in a first-transition-series compound, and an instance of rarely encountered Co(III) in a strictly four-coordinate planar environment.[10] Indeed, as observed earlier,[3,4] this is the structurally most diverse set of homoleptic complexes yet characterized.

While the solid-state structural aspects of the edt complexes have been satisfactorily exposed, little is known of their reactivity properties. Matters of interest include the stability of binuclear structures in solution, electron-transfer capabilities of mono- and binuclear species, the potential nucleophilic reactivity of sulfur atoms in the template synthesis of new ligand types, and the preparation of bridged polynuclear complexes. Earlier we had shown that $[Mn_2(edt)_4]^{2-}$ (partially) dissociates in solution and that the solution species exhibited unexpectedly large peak potential separations in cyclic voltammetry.[1] Similar behavior has been noted by others.[6,11] Additionally, $[Mn(edt)_2(HIm)]^-$ has been isolated from a DMF solution prepared from $[Mn_2(edt)_4]^{2-}$ and containing excess imidazole and shown to have a pyramidal structure.[12] These observations furnish the starting point for the examination of the solution equilibria and electrochemical features of first-transition-series edt complexes, the results of which are reported herein.

Experimental Section

Preparation of Compounds. The following compounds were prepared by published methods: $(Et_4N)_2[Ti(edt)_3]$,[3,4] $(Et_4N)_2[V_2(edt)_4]$,[2,4] $(Et_4N)_2[Cr(edt)_2]$,[3,4] $(Et_4N)_2[Mn_2(edt)_4]$,[1] $(n\text{-}Bu_4N)_2[Fe_2(edt)_4]$,[13] $(Ph_4P)_2[Mn(tdt)_2]\cdot 2MeOH$,[11] $(Ph_4P)_2[Mn(tdt)_2][Mn(tdt)_2(MeOH)]\cdot 3MeOH$,[11] $(n\text{-}Bu_4N)[Fe(tdt)_2]$,[14] $(n\text{-}Bu_4N)[Co(tdt)_2]$[14] (tdt = toluene-3,4-dithiolate).

Physical Measurements. All measurements were conducted under strictly anaerobic conditions; solvents were degassed immediately before use.

(a) Electrochemistry. Experiments were conducted on a PAR M-370 system. Potentials are reported at ~25 °C relative to a SCE reference electrode and are uncorrected for junction potentials. The reference electrode was checked periodically against 1.0 mM ferrocene solutions in the solvents of interest. The Fc^+/Fc potentials were 0.40 V (MeCN), 0.47 V (DMF, Me_2SO), and 0.45 V (CH_2Cl_2). Solvents were purified by standard procedures. A sealed all-glass cell was used; measurements were made under a pure dinitrogen atmosphere. The auxiliary electrode, which consisted of a platinum flag sealed in soft glass, and the reference electrode were separated from the working solution by means of a fritted bridge filled with the same solvent and supporting electrolyte. The solution in the reference electrode bridge was changed when necessary to prevent aqueous contamination of the solution. Uncompensated solution resistance in the cell configuration was minimized by placing the reference electrode tip as close to the working electrode as possible and using an approximately constant ratio of $(n\text{-}Bu_4N)ClO_4$ supporting electrolyte and solute concentration (~200:1). In acetonitrile and Me_2SO solutions at scan rates of 5–500 mV/s, the latter condition was found to be optimal for the reversibility (ΔE_p = 60 mV) of the Fc^+/Fc couple. Positive-feedback IR compensation was not used.

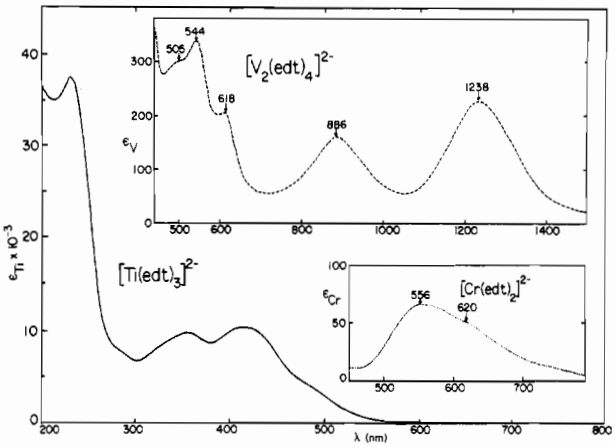

Figure 1. UV/visible absorption spectrum of $[Ti(edt)_3]^{2-}$ in acetonitrile and visible spectra of $[V_2(edt)_4]^{2-}$ and $[Cr(edt)_2]^{2-}$ in acetonitrile and DMF, respectively.

The working electrodes for cyclic voltammetry (CV) were glassy carbon, a platinum disk sealed in soft glass, and a pyrolytic graphite disk. The glassy-carbon electrode was pretreated by polishing with a gem-polish slurry on a felt cloth followed by rinsing with deionized water and drying. The platinum electrode was cleaned by immersion in 6 N HNO_3, rinsing with deionized water and then with acetone, and drying. The pyrolytic graphite electrode was constructed according to the procedure of Oyama and Anson.[15] The mounted graphite disks were cleaned by cutting off a thin section of the disk and the polyethylene supporting sheath with a scalpel. Careful attention was paid to electrode pretreatment before measurements in order to identify effects due to different electrodes and their surface properties. Platinum gauze was used as the working electrode in coulometry, which employed a PAR 179 digital coulometer. Cyclic voltammograms measured at scan rates >500 mV/s were recorded oscillographically. Differential pulse polarography was carried out with a glassy-carbon working electrode, peak-to-peak modulation amplitude of 25 mV, 2 pulses/s, and a scan rate of 5 mV/s. Single- and double-step chronoamperometry were performed by using a PAR 173 potentiostat, the preceding coulometer, and a PAR 377A cell system, in conjunction with a Houston Instruments 2000 XY recorder.

(b) Magnetic Susceptibilities. Magnetic properties in solution were determined by the usual NMR method[16a] with coaxial tubes, Me_4Si as the reference, and a Brüker WM-300 spectrometer operating at 300 MHz. Solvent susceptibilities[16b] and diamagnetic corrections[16c] were taken from literature tabulations.

(c) Absorption Spectra. Spectra were recorded on a Cary 219 or 2300 spectrophotometer. The following λ_{max} (ϵ_M) results were obtained. $[Ti(edt)_3]^{2-}$: 230 (38 900), 276 (sh, 8480), 355 (9810), 414 (10 400), 476 (sh, 4570) nm (MeCN). $[V_2(edt)_4]^{2-}$: 312 (sh, 6110), 368 (6920), 505 (300), 544 (340), 618 (205), 886 (160), 1238 (225) nm (MeCN). $[Cr(edt)_2]^{2-}$: 278 (sh, 10 800), 300 (sh, 8700), 556 (67), 620 (sh, 52) nm (DMF). $[Mn_2(edt)_4]^{2-}$: 320 (sh, 7560), 356 (10 900), 388 (sh, 7850), 640 (580) nm (MeCN, 7.02 mM); 290 (6490), 350 (16 100), 398 (10 200), 600 (1250) nm (Me_2SO, 4.72 mM); 328 (sh), 356, 400 (sh) nm (CH_2Cl_2, 1.3 mM). $[Fe_2(edt)_4]^{2-}$: 330 (sh, 7300), 374 (9170), 566 (2650), 620 (sh, 2100) nm (MeCN, 4.90 mM); 374 (12 200), 528 (3660), 580 (sh, 2600) nm (Me_2SO, 4.46 mM). $[Co(edt)_2]^{2-}$: 310 (8600), 380 (1890), 390 (1920), 420 (2370), 672 (420), 1200 (100) nm (MeCN). $[Co(edt)_2]^-$: 336 (9700), 364 (8330), 500 (sh, 680), 682 (3300), 720 (sh, 1880), 880 (sh, 225), 916 (sh, 250), 960 (270) nm (MeCN). Extinction

(2) Dorfman, J. R.; Holm, R. H. *Inorg. Chem.* **1983**, *22*, 3179.
(3) Dorfman, J. R.; Rao, Ch. Pulla; Holm, R. H. *Inorg. Chem.* **1985**, *24*, 453.
(4) Rao, Ch. Pulla; Dorfman, J. R.; Holm, R. H. *Inorg. Chem.* **1986**, *25*, 428.
(5) Szeymies, D.; Krebs, B.; Henkel, G. *Angew. Chem., Int. Ed. Engl.* **1983**, *22*, 885.
(6) Christou, G.; Huffman, J. C. *J. Chem. Soc., Chem. Commun.* **1983**, 558.
(7) (a) Wiggins, R. W.; Huffman, J. C.; Christou, G. *J. Chem. Soc., Chem. Commun.* **1983**, 1313. (b) Money, J. K.; Huffman, J. C.; Christou, G. *Inorg. Chem.* **1985**, *24*, 3297.
(8) Szeymies, D.; Krebs, B.; Henkel, G. *Angew. Chem., Int. Ed. Engl.* **1984**, *23*, 804.
(9) Snow, M. R.; Ibers, J. A. *Inorg. Chem.* **1973**, *12*, 249.
(10) A further example, $[Co(S\text{-}2,4,6\text{-}i\text{-}Pr_3C_6H_2)_4]^-$, has recently been described: Fikar, R.; Koch, S. A.; Millar, M. M. *Inorg. Chem.* **1985**, *24*, 3311.
(11) Henkel, G.; Greiwe, K.; Krebs, B. *Angew. Chem., Int. Ed. Engl.* **1985**, *24*, 117.
(12) Seela, J. L.; Huffman, J. C.; Christou, G. *J. Chem. Soc., Chem. Commun.* **1985**, 58.
(13) Herskovitz, T.; DePamphilis, B. V.; Gillum, W. O.; Holm, R. H. *Inorg. Chem.* **1975**, *14*, 1426.
(14) Williams, R.; Billig, E.; Waters, J. H.; Gray, H. B. *J. Am. Chem. Soc.* **1966**, *88*, 43.
(15) Oyama, N.; Anson, F. C. *J. Am. Chem. Soc.* **1979**, *101*, 3450.
(16) (a) Phillips, W. D.; Poe, M. *Methods Enzymol.* **1972**, *24*, 304. (b) Gerger, W.; Mayer, U.; Gutmann, V. *Monatsh. Chem.* **1977**, *108*, 417. (c) O'Connor, C. J. *Prog. Inorg. Chem.* **1982**, *29*, 203.

Table I. Electrochemical Properties of Complexes

complex	solvent	cyclic voltammetry[a] [M], mM	cyclic voltammetry[a] $E_{1/2}$ (ΔE_p),[b] V	coulometry process	coulometry n/M[g]
$[Ti(edt)_3]^{2-}$	MeCN	3.09	−2.09[c]	red	≳2.7
$[V_2(edt)_4]^{2-}$	MeCN	4.64	−0.61 (70)	ox	0.49
$[Cr(edt)_2]^{2-}$	DMF	2.88	−1.00[d,e]	ox	0.50
$[Mn(edt)_2]^{2-}$	Me_2SO	3.29	−0.88 (150)	ox	0.82
	MeCN	2.05	−0.89 (120)		
$[Mn_2(edt)_4]^{2-}$	Me_2SO	20.4	−0.86 (120)	red	1.09
		7.34	−0.90 (190)		
		1.46	−0.93 (330)		
	MeCN	10.2	−0.94 (130)	red	1.10
		4.25	−0.91 (140)		
		2.06	−0.95 (170)		
	CH_2Cl_2	~1.1	−0.92 (210)		
$[Fe_2(edt)_4]^{2-}$	Me_2SO	8.35	−1.03 (80)	red	1.07
		2.90	−1.06 (60)		
		1.02	−1.05 (70)		
	MeCN	3.99	−1.13 (100)	red	1.10
$[Fe(edt)_2]^{2-}$[f]	MeCN	3.99	−1.12 (80)		
$[Co(edt)_2]^{-}$ + $[Co(edt)_2]^{2-}$	MeCN	2.84	−1.16 (60)	ox	0.55
				red	0.53
$[Mn(tdt)_2]^{2-}$	Me_2SO	0.45	−0.76 (150)		
$[Mn(tdt)_2]^{-}$	DMF	3.33	−0.72 (110)		
$[Fe(tdt)_2]^{-}$	Me_2SO	3.99	−0.92 (70)		
	MeCN	4.72	−0.91 (60)	red	1.10
$[Co(tdt)_2]^{-}$	Me_2SO	0.89	−0.78 (60)		

[a] Glassy-carbon working electrode; scan rate 50 mV/s unless noted otherwise. [b] $E_{1/2} = (E_{p,a} + E_{p,c})/2$; ΔE_p in mV. [c] Irreversible, $E_{p,c}$. [d] Irreversible, $E_{p,a}$. [e] 200 mV/s. [f] Electrochemically generated. [g] Number of electrons passed per metal atom.

Table II. Magnetic Moments of V(III), Cr(II), Mn(II), and Fe(III) Complexes in Solution and Solid Phases at 297 K

complex	solvent	[M], mM	μ_M, μ_B	N_m
$[V_2(edt)_4]^{2-}$	CD_3CN	4.86–34.5	0.88 (10)[a]	
$[Cr(edt)_2]^{2-}$	CD_3CN	31.5	4.95	
$[Mn_2(edt)_4]^{2-}$[e]	$(CD_3)_2SO$	1.49	5.12	1.10
		2.62	4.89	0.78
		7.37	5.01	0.89
		19.5	4.88	0.77
		56.2	4.65	0.56
		127.8	4.57	0.49
	CD_3CN	2.00	4.60	0.52
		4.01	4.31	0.28
		6.98	4.15	0.15
		20.0	4.04	0.06
	solid[c]		3.96	
$[Fe_2(edt)_4]^{2-}$[e]	CD_3CN	1.96–16.7	2.57 (6)[b]	0
	$(CD_3)_2SO$	1.12	3.47	0.57 (0.19)[f]
		2.19	3.38	0.51 (0.17)
		4.18	3.37	0.50 (0.16)
		4.68	3.22	0.39 (0.13)
		6.68	3.22	0.39 (0.13)
		10.9	3.07	0.29 (0.10)
		16.1	3.02	0.26 (0.09)
		19.5	3.08	0.30 (0.10)
		20.9	2.93	0.20 (0.07)
		23.4	2.89	0.18 (0.06)
	solid[d]		2.59	

[a] Standard deviation of the mean of four values. [b] Standard deviation of the mean of eight values. [c] Et_4N^+ salt.[1] [d] n-Bu_4N^+ salt at 287 K.[13] Magnetic moments of solids are uncorrected for interanion magnetic interactions. [e] Formula does not imply exclusive dimeric species in solution. [f] Values for $S = {}^3/_2$ (${}^5/_2$).

coefficients, concentrations, and coulometric n values are given on a per metal basis. $[Co(edt)_2]^-$ and $[Co(edt)_2]^{2-}$ were electrochemically generated, and their spectra were measured in situ. Extinction coefficients of $[Mn_2(edt)_4]^{2-}$ given here are to be preferred to those given earlier,[1] certain of which are incorrect.

^1H NMR spectra were recorded at 300 MHz on a Brüker WM-300 spectrometer; chemical shifts are downfield relative to Me_4Si internal standard.

Results and Discussion

The spectral, structural, and equilibrium behavior and the redox properties of edt complexes of Ti(IV), V(III), Cr(II), Mn(II,III),

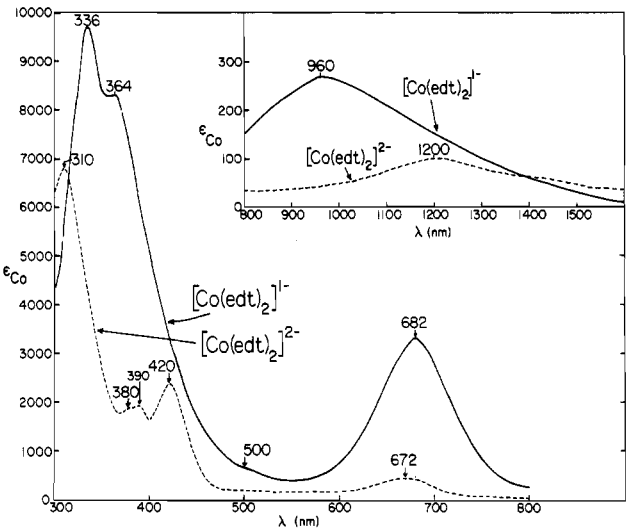

Figure 2. Absorption spectra of electrochemically generated $[Co(edt)_2]^-$ and $[Co(edt)_2]^{2-}$ in acetonitrile.

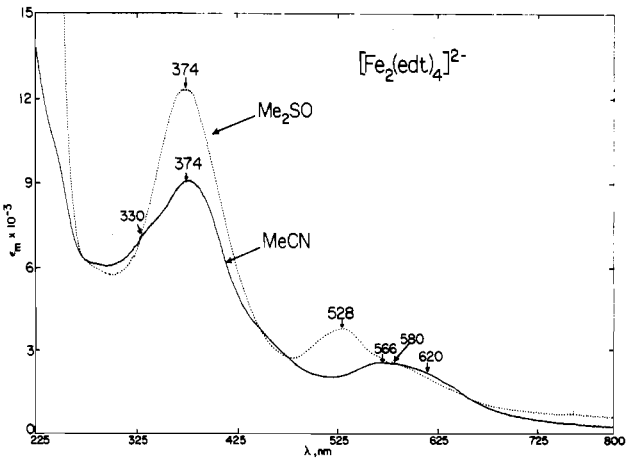

Figure 3. Absorption spectra of Me_2SO (4.46 mM) and acetonitrile (4.90 mM) solutions prepared from $[Fe_2(edt)_4]^{2-}$.

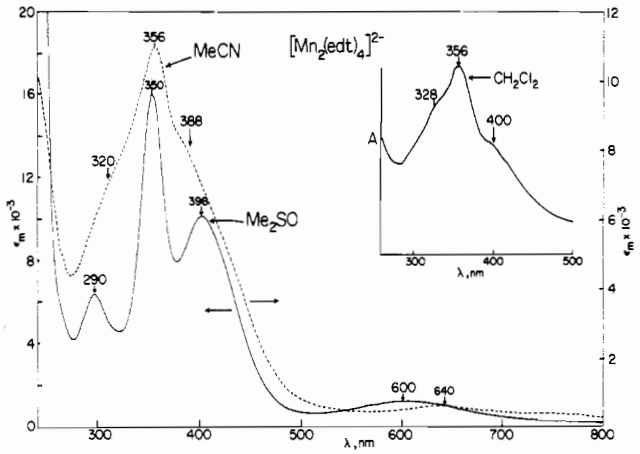

Figure 4. Absorption spectra of Me_2SO (4.72 mM), acetonitrile (7.02 mM), and dichloromethane (~1.3 mM) solutions prepared from $[Mn_2(edt)_4]^{2-}$.

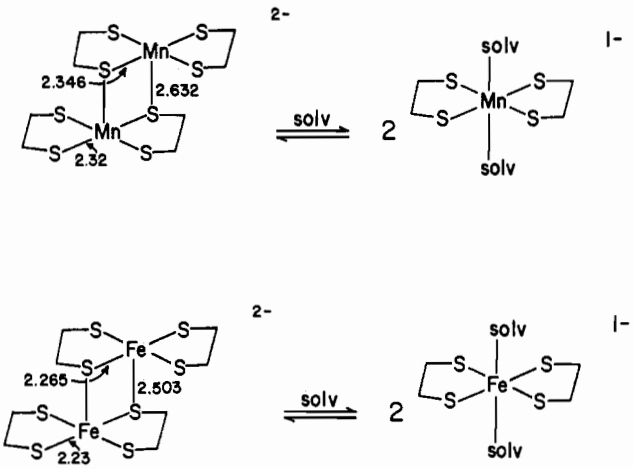

Figure 5. Schematic depiction of species involved in dimer 2–monomer equilibria. Bond distances (Å) for $[M_2(edt)_4]^{2-}$ are given; terminal M–S distances are mean values.

Fe(II,III), and Co(II,III) have been examined in solution. Electrochemical and magnetic data are collected in Tables I and II. Absorption spectra, which are characteristic and provide the simplest means of compound identification, are presented in Figures 1–4. Structures of all complexes considered below have been described in detail elsewhere.[1-9]

Mononuclear Complexes. (a) $[Ti(edt)_3]^{2-}$. This species has a trigonally distorted octahedral configuration in the solid state and is the only $(edt)_3$ complex of the first transition series yet isolated (vide infra). It is likely that in this series the +4 oxidation state is required to afford M–S interactions sufficiently stable to override ligand–ligand repulsion.[17] The latter will be enhanced owing to the size of thiolate sulfur atoms and the small saturated nature of the ligand, which requires that essentially all negative charge be located on those atoms in the free ligand. The complex forms red-orange solutions with a rich LMCT spectrum (Figure 1). $[Ti(edt)_3]^{2-}$ is irreversibly reduced at a very negative potential ($E_{p,c} = -2.09$ V). Under coulometric conditions in acetonitrile, the solution color becomes yellow upon passage of 1 faraday. The orange color of $[Ti(edt)_3]^{2-}$ is not recovered upon oxidation of the yellow solution. Further reduction of this solution produces turbidity. These observations indicate the instability of the initial reduction product of $[Ti(edt)_3]^{2-}$, which is presumably $[Ti(edt)_3]^{3-}$.

(b) $[Cr(edt)_2]^{2-}$. This is the only discrete Cr thiolate complex yet prepared[18] and one of the few structurally characterized molecular Cr(II) species, all of which are planar. The others are $Cr[H_2B(pz)_2]_2$,[19] $Cr(acac)_2$,[20] and $Cr[N(SiMe_3)_2]_2(THF)_2$.[21] This complex forms violet solutions that are extremely sensitive to oxidation. The magnetic moment of 4.95 μ_B in acetonitrile at 297 K demonstrates the high-spin d^4 configuration. The paramagnetism causes the chemical shift of ligand protons at 46 ppm. Two ligand field transitions, at 620 (sh) and 556 nm and of $^5E_g \rightarrow {}^5T_{2g}$ octahedral parentage, are detectable (Figure 1). From the sparse data available for planar Cr(II) chromophores,[19,21-23] it appears that thiolate affords a weaker ligand field than β-diketonates[22] and β-ketoaminates,[23] consistent with the usual position of thiolate vs. nitrogen and anionic oxygen ligands in the spectrochemical series. In DMF solution $[Cr(edt)_2]^{2-}$ is irreversibly oxidized at $E_{p,a} = -1.00$ V. Coulometry indicates the passage of 0.5 e^-/Cr. The oxidation product has not been isolated, and the reason for this low value of n is unknown.

(c) $[Co(edt)_2]^{2-}$ and $[Co(edt)_2]^-$. We have previously shown[4] that the crystalline solid of composition $(Me_4N)_3[Co_2(edt)_4]$ contains a 1:1 mixture of *tetrahedral* $[Co(edt)_2]^{2-}$ and *planar* $[Co(edt)_2]^-$. These species have not yet been separately prepared. This composition is retained in solution. If the magnetic moment of 4.6 μ_B, known for other tetrahedral $[Co(SR)_4]^{2-}$ species,[24] is assumed for $[Co(edt)_2]^{2-}$, the experimental value of 3.80 μ_B/Co in acetonitrile at 297 K corresponds to 2.8 μ_B, or a triplet ground state, for $[Co(edt)_2]^-$. In this solvent the solution species exhibited a fully reversible redox process at $E_{1/2} = -1.16$ V. Coulometry at potentials of −1.6 and −0.6 V resulted in passage of very close to $n = 0.5$ in each case, indicating that half of the cobalt is reduced and oxidized, respectively, at these potentials. Cyclic voltammetry of the oxidized and reduced solutions after coulometry displayed identical behavior, indicating stability of the redox products. The ^1H NMR spectrum contained two isotropically shifted, broad signals of roughly equal intensity at 174 and 246 ppm. The latter was abolished upon addition of the oxidant $(Cp_2Fe)(BF_4)$ and is thus assigned to $[Co(edt)_2]^{2-}$. Absorption spectra of solutions resulting from controlled-potential electrolysis are shown in Figure 2. At −1.6 V, the green color of the original solution lightens and the spectrum of $[Co(edt)_2]^{2-}$, clearly similar to those of other tetrahedral Co(II) thiolate chromophores,[24-26] is evident. The features at 1200 and 672 nm correspond to the ν_2 and ν_3 bands of tetrahedral Co(II), respectively, and the LMCT bands near 400 nm are also characteristic of this chromophore type.

Electrolysis at −0.6 V caused the solution to become dark green as the intense spectrum of $[Co(edt)_2]^-$ developed. The most distinctive features, at 682 and 960 nm, increased simultaneously in intensity as the electrolysis proceeded. The former is certainly a LMCT band while the latter, which appears to possibly have a counterpart at ~900 nm in the spectra of bis(biuretato)Co(III) complexes,[27] is apparently a d–d band.[28]

(17) The only other $(edt)_3$ complexes are $[M(edt)_3]^-$ (M = Nb(V), Ta(V)), which we learned of after completion of the present work: Tatsumi, K.; Sekiguchi, Y.; Nakamura, A.; Cramer, R. E.; Rupp, J. J. *Angew. Chem., Int. Ed. Engl.* **1986**, *25*, 86.
(18) The Cr(III) thiolate–alkoxide complex $[Cr_3(SCH_2CH_2O)_6]^{3-}$ has recently been prepared: Nicholson, J. R.; Wang, R.-J.; Huffman, J. C.; Christou, G.; Chang, H.-R.; Hendrickson, D. N. *J. Chem. Soc., Chem. Commun.* **1985**, 1781.
(19) Dapporto, P.; Mani, F.; Mealli, C. *Inorg. Chem.* **1978**, *17*, 1323.
(20) Cotton, F. A.; Rice, C. E.; Rice, G. W. *Inorg. Chim. Acta* **1977**, *24*, 231.
(21) Bradley, D. C.; Hursthouse, M. B.; Newing, C. W.; Welch, A. J. *J. Chem. Soc., Chem. Commun.* **1972**, 567.
(22) Gerlach, D. H.; Holm, R. H. *Inorg. Chem.* **1969**, *8*, 2292.
(23) Gerlach, D. H.; Holm, R. H. *Inorg. Chem.* **1970**, *9*, 588.
(24) Lane, R. W.; Ibers, J. A.; Frankel, R. B.; Papaefthymiou, G. C.; Holm, R. H. *J. Am. Chem. Soc.* **1977**, *99*, 84.
(25) Nakata, M.; Ueyama, N.; Nakamura, A.; Nozawa, T.; Hatano, M. *Inorg. Chem.* **1983**, *22*, 3028.
(26) Hagen, K. S.; Holm, R. H. *Inorg. Chem.* **1984**, *23*, 418.
(27) (a) Bour, J. J.; Beurskens, P. T.; Steggerda, J. J. *J. Chem. Soc., Chem. Commun.* **1972**, 221. (b) Birker, P. J. W. M. L.; Bour, J. J.; Steggerda, J. J. *Inorg. Chem.* **1973**, *12*, 1255.
(28) Other examples of (the few) planar spin-triplet Co(III) complexes known derive from deprotonated biuret[27] and dithiolene[14,29] ligands. Of the entire set, $[Co(edt)_2]^-$ (green) and $[Co(S\text{-}2,4,6\text{-}i\text{-}Pr_3C_6H_2)_4]^-$[10] (red) would be expected to be the most similar. Their visible LMCT spectra are, however, rather different.
(29) (a) Baker-Hawkes, M. J.; Billig, E.; Gray, H. B. *J. Am. Chem. Soc.* **1966**, *88*, 4870. (b) Hoyer, E.; Dietzsch, W.; Müller, H.; Schroth, W. *Z. Chem.* **1967**, *7*, 354. (c) van der Put, P. J.; Schilperoord, A. A. *Inorg. Chem.* **1974**, *13*, 2476. (d) Davison, A.; Edelstein, N.; Holm, R. H.; Maki, A. H. *Ibid.* **1963**, *2*, 1227; **1964**, *3*, 814.

A different Co(III)–edt compound, $Na_3[Co(edt)_3]\cdot 2H_2O$, formed in the reaction of neat H_2edt and $Na_3[Co(CO_3)_3]\cdot 3H_2O$, had been claimed in 1960.[30] The formulation was based on elemental analysis only. Repetition of the procedure did give a black precipitate, as described. This, however, was insoluble in all common solvents, and its analysis deviated markedly from that of the indicated formulation.[31] We are disinclined to accept the existence of $[Co(edt)_3]^{3-}$.

Binuclear Complexes. The species $[M_2(edt)_4]^{2-}$ exist in two configurations, the quadruply bridged form **1** (M = V(III)) and the lateral, doubly bridged form **2** (M = Fe(III), Mn(III)). A

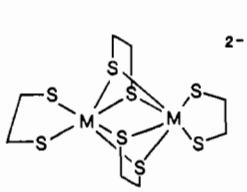

1

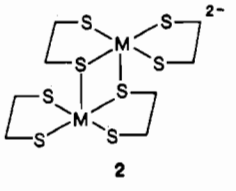

2

matter of obvious importance is the structure of the intermediate member, $[Cr_2(edt)_4]^{2-}$, of this series. Extended Hückel calculations indicate that dimer **1** is unlikely to be stable for M(III) d^n ions with $n \geq 4$ owing to the occupation of antibonding orbitals.[4] Unfortunately, we have not yet been able to crystallize any polynuclear Cr(III)–edt complex[4] in a form suitable for X-ray structure determination. A significant aspect of the solution chemistry of the binuclear complexes is their tendency to dissociate, a matter illustrated for **2** in Figure 5, which also includes bridging and terminal bond distances.[1,9]

(a) $[V_2(edt)_4]^{2-}$. This complex is very weakly paramagnetic in the solid state and in acetonitrile solution, where it shows a concentration-independent moment of 0.88 ± 0.10 μ_B at 297 K. This is interpreted to indicate nil dissociation. The paramagnetism presumably derives from a low-lying triplet state, whose existence is suggested by extended Hückel results.[4] The absorption spectrum (Figure 1) exhibits a set of relatively weak visible and near-IR bands that must be associated with structure **1** but are otherwise unassigned. The ^1H NMR spectrum contains a single broad isotropically shifted signal at 4.08 ppm; no other resonances could be detected in the interval of ±200 ppm from Me_4Si. $[V_2(edt)_4]^{2-}$ is oxidized in a reversible process at $E_{1/2}$ = –0.61 V with n = 0.5 in acetonitrile, where a color change from red-brown to dark brown occurs. However, the oxidized species did not persist as $[V_2(edt)_4]^-$ after completion of coulometry (20–30 min) inasmuch as the dark brown solution lacked the –0.6 V response in cyclic voltammetry.

The solution behavior of $[Fe_2(edt)_4]^{2-}$ and $[Mn_2(edt)_4]^{2-}$ is examined in the following two subsections. Spectra of solutions prepared from salts of these dimers differ appreciably in weakly coordinating (acetonitrile) and strongly coordinating (Me_2SO) solvents, indicating the existence of at least two species. However, these spectra overlap considerably, and ^1H NMR spectra contain extremely broad resonances that are not useful for detection of individual species. This matter is better pursued by means of magnetic susceptibility measurements. The results in Table II, withdrawn from a larger data set, reveal the concentration dependence of magnetic moment μ_M per metal atom. Measurements were extended to near the solubility limit in acetonitrile and Me_2SO. Reliable moments could not be determined in dichloromethane, where dimer dissociation is improbable, owing to low solubility and/or decomposition. A concentration dependence is observed in all systems except $[Fe_2(edt)_4]^{2-}$ in acetonitrile. Values of μ_M increase with decreasing dimer concentration, consistent with equilibrium 1 (Figure 5) in which solvated

$$[M_2(edt)_4]^{2-} + 4solv \rightleftharpoons 2[M(edt)_2(solv)_2]^- \qquad (1)$$

monomeric complexes (m) coexist with antiferromagnetically coupled dimers (d) having lower μ_M values. The monomers are depicted somewhat arbitrarily as tetragonal *di*solvates. For reaction 1, $K_{eq} = [m]^2/[d] = 4x^2/(C - x)$. It can be shown that the mole fraction of monomer, N_m, and the equilibrium quotient are given by eq 2 and 3, respectively, where the observed magnetic moment $\mu_{obsd} = \mu_M$. Values of N_m calculated from magnetic data are included in Table II.

$$N_m = (\mu_{obsd}^2 - \mu_d^2)/(\mu_m^2 - \mu_d^2) \qquad (2)$$

$$K_{eq} = \frac{2C(\mu_{obsd}^2 - \mu_d^2)}{(\mu_{obsd}^2 - 2\mu_m^2 + \mu_d^2)(\mu_{obsd}^2 - \mu_m^2)} \qquad (3)$$

(b) $[Fe_2(edt)_4]^{2-}$. This species in acetonitrile at [Fe] = 2–17 mM exhibits a concentration-independent magnetic moment μ_M = 2.57 ± 0.06 μ_B. This value is indistinguishable from μ_d = 2.59 μ_B for the crystalline n-Bu_4N^+ salt at 287 K.[13] Consequently, $[Fe_2(edt)_4]^{2-}$ is not dissociated to a detectable extent in acetonitrile, and the spectrum in this solvent (Figure 3) is that of the intact dimer.

In Me_2SO solution the situation is quite different inasmuch as μ_M decreases from 3.47 to 2.89 μ_B at [Fe] = 1–23 mM. Calculations of K_{eq} and N_m require an assumption of $S = {}^3/_2$ or ${}^5/_2$ for the mononuclear complex. Values of these quantities that follow are written as those for $S = {}^3/_2$ (${}^5/_2$). The possibility of the intermediate spin state is raised by the quartet states of Fe$(S_2CNR_2)_2X$,[32,33] solution moments of 3.87 μ_B (Me_2SO) and 4.03 μ_B (pyridine) for $[Fe(tdt)_2]^-$,[14] and μ = 3.87 μ_B for isolated (n-Bu_4N)[Fe(mnt)$_2$(pip)][34] (pip = piperidine). The limiting values μ_m = 5.92 and 4.00 μ_B correspond to the spin-only moment for $S = {}^5/_2$ and the ambient-temperature moment of Fe$(S_2CNEt_2)_2Cl$,[32a] respectively. With use of these values and of μ_d above, N_m was found to decrease from 0.57 (0.19) to 0.18 (0.06) as the concentration is increased, and $K_{eq} \approx$ 1.7 (4) (0.12 (4)) mM. These and subsequent results must be considered as good estimates but not quantitative determinations owing to the experimental error in μ_M (±0.05 μ_B), as well as the uncertainty in monomer and dimer limiting moments. The calculated equilibrium constants are extremely sensitive to these values. The spectral feature characteristic of the solvated monomer is the band at 528 nm (Figure 3); at the concentration of the solution used, $N_m \sim$ 0.5 (0.1).

Dimer–monomer equilibria similar to reaction 1 have been detected for Fe–dithiolene complexes,[34–36] whose dimeric structures[36,37] are analogous to **2**. Among these is $[Fe_2(tdt)_4]^{2-}$ as its Et_4N^+ and n-Bu_4N^+ salts.[37c,d] On the basis of its magnetic[14] and, to a lesser extent, conductivity[35] properties, this dimer is completely dissociated in acetonitrile and Me_2SO. In electrochemical experiments (vide infra) $[Fe(tdt)_2]^-$ is taken as a n = 1 current standard.

(c) $[Mn_2(edt)_4]^{2-}$. Dilute solutions in Me_2SO ([Mn] $\lesssim$ 3 mM) show $\mu_M > 4.88$ μ_B, the spin-only value for high-spin d^4. From the most dilute solution the value μ_m = 5.12 μ_B is taken, and from solid-state magnetism[38] μ_d = 3.96 μ_B. Consequently, N_m decreases

(30) Bauer, H. F.; Drinkard, W. C. *J. Am. Chem. Soc.* **1960**, *82*, 5031.
(31) Anal. Found: C, 4.17; H, 0.60; Co, 51.74; S, 15.75.

(32) (a) Martin, R. L.; White, A. H. *Inorg. Chem.* **1967**, *6*, 712. (b) Chapps, G. E.; McCann, S. W.; Wickman, H. H.; Sherwood, R. C. *J. Chem. Phys.* **1974**, *60*, 990.
(33) The magnetic susceptibility behavior of antiferromagnetic (n-$Bu_4N)_2$[Fe_2(edt)$_4$], which contains two identical distorted square-pyramidal sites,[9] has been interpreted as marginally favoring two $S = {}^5/_2$ Fe(III) ions.[13] As observed,[13] the behavior of this and the $S = {}^3/_2$ case are only slightly different in the temperature interval of measurement, and the quadrupole splitting is large for high-spin Fe(III). The results of extended Hückel calculations[4] are consistent with $S = {}^3/_2$ states. These factors further emphasize the possibility of a quartet state for solvated $[Fe(edt)_2]^-$.
(34) Dance, I. G.; Miller, T. R. *Inorg. Chem.* **1974**, *13*, 525. mnt = maleonitriledithiolate.
(35) Balch, A. L.; Dance, I. G.; Holm, R. H. *J. Am. Chem. Soc.* **1968**, *90*, 1139.
(36) Kanatzidis, M.; Coucouvanis, D. *Inorg. Chem.* **1984**, *23*, 403.
(37) (a) Hamilton, W. C.; Bernal, I. *Inorg. Chem.* **1967**, *6*, 2003. (b) Schultz, A. J.; Eisenberg, R. *Ibid.* **1973**, *12*, 518. (c) Henkel, G.; Tremel, W.; Kuhlmann, U.; Krebs, B. *Abstracts*, 21st International Conference on Coordination Chemistry, Toulouse, France, 1980; p 351. (d) Sawyer, D. T.; Srivatsa, G. S.; Bodini, M. E.; Schaefer, W. P.; Wing, R. M. *J. Am. Chem. Soc.* **1986**, *108*, 936.
(38) Dorfman, J. R.; Hatfield, W. E.; ter Haar, L. W.; Holm, R. H., unpublished results.

Table III. Cyclic Voltammetry of $[Fe_2(edt)_4]^{2-}$ in Acetonitrile Solution at ~25 °C (Glassy-Carbon Electrode, [Fe] = 4 mM)

v, V/s	$E_{p,c}$[a]	$E_{p,a}$[a]	$i_{p,a}/i_{p,c}$	$E_{1/2}$[a] (ΔE_p,[b] mV)	$i_{p,c}/v^{1/2}C$[c]
0.005	−1.16	−1.10	0.96	−1.13 (60)	0.40
0.020	−1.17	−1.09	1.02	−1.13 (80)	0.36
0.050	−1.18	−1.08	1.09	−1.13 (100)	0.31
0.100	−1.18	−1.07	1.15	−1.13 (110)	0.30
0.200	−1.19	−1.06	1.11	−1.13 (130)	0.27
0.500	−1.20	−1.04	1.18	−1.12 (160)	0.22
1.00	−1.21	−1.04	1.46	−1.13 (170)	0.16
2.00	−1.23, −1.44	−1.03	1.6[d]	−1.13 (200)	0.13[e]
5.00	−1.25, −1.49	−0.99	1.7[d]	−1.12 (260)	0.10[e]
10.00	−1.25, −1.56	−0.96	1.9[d]	−1.11 (290)	0.08[e]

[a] V vs. SCE. [b] $\Delta E_p = E_{p,a} - E_{p,c}$. [c] mA $V^{-1/2}$ $s^{1/2}$ mM^{-1}; C = [dimer]. [d] $i_{p,a}/i_{p,c1}$ at ≥2 V/s. [e] Evaluated from $i_{p,c1}$ at ≥2 V/s.

from 1.0 at 1.5 mM to 0.49 at 128 mM (Table II). For equilibrium 1, $K_{eq} \approx 81$ (18) mM. In acetonitrile at [Mn] = 2 mM, $N_m \cong 0.52$ and decreases to 0.06 at 20 mM. As reported earlier,[1] absorption spectra are solvent-dependent. The spectrum in dichloromethane (Figure 4) is that of intact $[Mn_2(edt)_4]^{2-}$; the spectrum in acetonitrile at a concentration corresponding to $N_m \sim 0.2$ is obviously very similar. In Me_2SO, where $N_m \sim 0.8$, the spectrum differs, and the maxima at 290, 398, and 600 nm are characteristic of the mononuclear species. These systems provide the first examples of equilibrium 1 for Mn(III). The only bis(dithiolene)manganese monoanions that have been isolated, $[Mn(tdt)_2]^-$ and $[Mn(tdt)_2(MeOH)]^-$,[11] are mononuclear in the solid state, as is $[Mn(edt)_2(HIm)]^-$.[42]

Electron-Transfer Properties of $[M_2(edt)_4]^{2-}$. (a) $[Fe_2(edt)_4]^{2-}$. All experiments in acetonitrile solution were carried out in the concentration range for which magnetic data (Table II) indicate the presence of dimer **2** only. Within this range electrochemical behavior was independent of concentration. Coulometry gave n = 1.1 for reduction at −1.5 V, which was accompanied by a color change from dark brown to light yellow, and n = 0.9 for reoxidation at −0.4 V. The cyclic voltammogram of a coulometrically fully reduced solution is the exact complement of that of the unreduced solution at the same scan rate. These observations demonstrate effective reversibility of overall reaction 4 in Scheme I. The complex $[Fe(edt)_2]^{2-}$ has not been isolated; its mononuclear formulation follows from its 2− charge. All other $[M(edt)_2]^{2-}$ species are mononuclear.[1,3,4] A tetrahedral structure is virtually certain on the basis of the stereochemical preference of Fe(II), which is expressed without exception in mono- and polynuclear Fe(II) thiolates.[24,26,39]

Scheme I

$$[Fe_2(edt)_4]^{2-} + 2e^- \overset{-1.13\ V}{\rightleftharpoons} 2[Fe(edt)_2]^{2-} \quad (4)$$

$$[Fe_2(edt)_4]^{2-} + n_5e^- \overset{E_5}{\rightleftharpoons} [Fe_2(edt)_4]^{3-} \quad (5)$$

$$[Fe_2(edt)_4]^{3-} + 2MeCN \overset{k_6}{\rightleftharpoons} [Fe(edt)_2(MeCN)_2]^- + [Fe(edt)_2]^{2-} \quad (6)$$

$$[Fe(edt)_2(MeCN)_2]^- + n_7e^- \overset{E_7}{\rightleftharpoons} [Fe(edt)_2]^{2-} + 2MeCN \quad (7)$$

$$[Fe(edt)_2(MeCN)_2]^- + [Fe_2(edt)_4]^{3-} \underset{k_b}{\overset{k_f}{\rightleftharpoons}} [Fe(edt)_2]^{2-} + [Fe_2(edt)_4]^{2-} + 2MeCN \quad (8)$$

$$[Fe_2(edt)_4]^{2-} \overset{-1.25\ V}{\underset{E_{p,c1}}{\leftrightarrow}} [Fe_2(edt)_4]^{3-} \overset{-1.56\ V}{\underset{E_{p,c2}}{\leftrightarrow}} 2[Fe(edt)_2]^{2-} \quad (9)$$

(10 V/s)

In cyclic voltammetry over the potential interval −0.4 to −1.8 V and at the scan rates v = 5–500 mV/s, a single redox process was observed with $E_{1/2}$ = −1.13 V. CV parameters over the full scan rate range of 0.005–10 V/s are collected in Table III. As seen in this table and in Figure 6, the peak current ratio $i_{p,a}/i_{p,c}$ is nearly unity at slow scan rates and the peak current functions $i_p/v^{1/2}C$, when compared with those for the one-electron standard $[Fe(tdt)_2]^-$ at the same scan rates, correspond to a *two*-electron process. Separate reduction steps were not detected by differential pulse polarography, which gave E_p = −1.12 V. The $[Fe(tdt)_2]^{2-,-}$ couple is electrochemically perfectly reversible. The following observations show that the electron-transfer behavior of $[Fe_2(edt)_4]^{2-}$ does not correspond to a reversible process for n = 2:[40,41] $\Delta E_p > 59/n$ mV, peak half-width >90/n mV; $|E_{p,c} - E_{p,c}/2| >$ 30 mV; nonindependence of ΔE_p, $i_{p,a}/i_{p,c}$, and $i_{p,c}/v^{1/2}C$ on v. Evidently, the rate of electron transfer is subject to kinetic constraints. Operation of a slow two-step charge transfer (EE mechanism[42-44]) with $E_2 > E_1$ is excluded because the pronounced decrease in current function with increasing scan rate indicates that the charge transfers are coupled to a homogeneous chemical reaction.

As the scan rate is increased to ≳0.5 V/s, the cathodic peak broadens and $i_{p,a}/i_{p,c}$ increases well above unity. At >1 V/s the cathodic peak splits into two incompletely resolved features. The less negative of these does not shift appreciably as v is increased whereas the more negative feature is cathodically shifted, until at 10 V/s $E_{p,c1}$ = −1.25 V, $E_{p,c2}$ = −1.56 V, and $i_{p,a}/i_{p,c1}$ = 1.9. This behavior is evident from the voltammograms in Figure 6. The $E_{p,c1}$ feature is more electrochemically reversible than is $E_{p,c2}$. The nearly 1:2 peak current ratio at the fastest scan rate suggests that $E_{p,c1}$ corresponds to a one-electron process, a point confirmed by the excellent agreement of $i_{p,c1}/v^{1/2}C$ vs. $v^{1/2}$ plots for this feature and $[Fe(tdt)_2]^-$.

The preceding observations can be rationalized as follows, with reference to the reactions of Scheme I. At low scan rates (≲0.5 V/s) $[Fe_2(edt)_4]^{2-}$ is reduced in one-electron reaction 5. The Fe(II,III) product then rapidly equilibrates in reaction 6. If it is assumed that the potential for reduction of $[Fe(edt)_2(MeCN)_2]^-$ is greater than ca. −1.13 V,[45] this species will be quickly reduced at the electrode in reaction 7. Otherwise, cross-reaction 8, in effect a disproportionation (DISP) of $[Fe_2(edt)_4]^{3-}$, may intercede. If we neglect this possibility for the moment, the reaction sum 5 + 6 + 7 = reaction 4 and the overall process follows an ECE mechanism.[41,46] Slow scans provide sufficient time for the completion of forward reaction 6. At faster scan rates (>1 V/s) this reaction competes less and less favorably with the rate of formation

(39) (a) Hagen, K. S.; Stephan, D. W.; Holm, R. H. *Inorg. Chem.* **1982**, *21*, 3928. (b) Henkel, G.; Tremel, W.; Krebs, B. *Angew. Chem., Int. Ed. Engl.* **1983**, *22*, 319. (c) Coucouvanis, D.; Swenson, D.; Baenziger, N. C.; Murphy, C.; Holah, D. G.; Sfarnas, N.; Simopoulos, A.; Kostikas, A. *J. Am. Chem. Soc.* **1981**, *103*, 3350.

(40) Parry, E. P.; Osteryoung, R. A. *Anal. Chem.* **1965**, *37*, 1634.

(41) Brown, E. R.; Large, R. F. In *Physical Methods of Chemistry. Part IIA. Electrochemical Methods*; Weissberger, A., Rossiter, B. W., Eds.; Wiley-Interscience: New York, 1971; Chapter VI.

(42) Polcyn, D. S.; Shain, I. *Anal. Chem.* **1966**, *38*, 370.

(43) Ryan, M. D. *J. Electrochem. Soc.* **1978**, *125*, 547.

(44) (a) Lemoine, P.; Giraudeau, A.; Gross, M. *Electrochim. Acta* **1976**, *21*, 1. (b) van der Linden, J. G. M.; Paulissen, M. L. H.; Schmitz, J. E. J. *J. Am. Chem. Soc.* **1983**, *105*, 1903. (c) Bowyer, W. J.; Geiger, W. E. *Ibid.* **1985**, *107*, 5657. (d) Tulyathan, B.; Geiger, W. E. *Ibid.* **1985**, *107*, 5960. These papers describe EE systems.

(45) In support of this assumption, the potentials of solutions prepared from $[M_2(edt)_4]^{2-}$ (Table I) are about the same or less negative for the most dilute Me_2SO solution (largest N_m) compared to the most concentrated acetonitrile solution (smallest N_m). With M = Fe(III) this difference is ~60 mV.

(46) Nicholson, R. S.; Shain, I. *Anal. Chem.* **1965**, *37*, 178, 190.

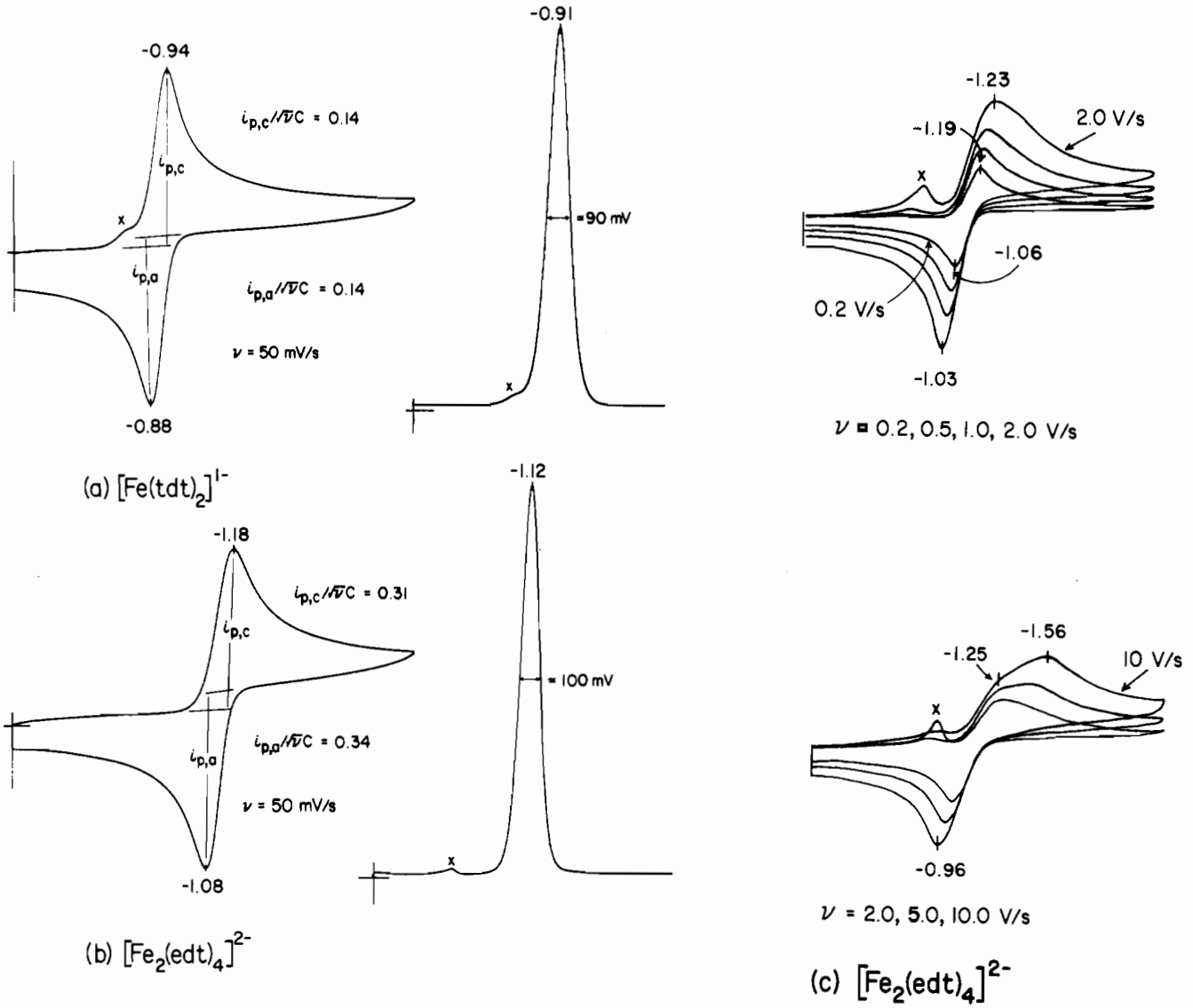

Figure 6. Cyclic voltammograms (50 mV/s, −0.4 to −1.8 V) and differential pulse polarograms of (a) $[Fe(tdt)_2]^-$ (4.72 mM) and (b) $[Fe_2(edt)_4]^{2-}$ ([Fe] = 3.99 mM) in acetonitrile solutions and cyclic voltammograms of (c) $[Fe_2(edt)_4]^{2-}$ ([Fe] = 14.3 mM) at 0.2–10 V/s in acetonitrile solution. A glassy-carbon working electrode was used for all measurements. Peak potentials are indicated; dimensions of the current function are mA $s^{1/2}$ $V^{-1/2}$ mM^{-1}. x = adsorbate feature.

of $[Fe_2(edt)_4]^{3-}$, resulting in a progressive decrease of the cathodic peak current toward the one-electron value at $E_{p,c1}$. When this situation is reached, the mixed-valence species is kinetically stable. The second cathodic event ($E_{p,c2}$) completes reduction sequence 9, whose net is reaction 4.

A pure ECE mechanism would involve reactions 5–7 only. If, however, $E_7 > E_5 = -1.13$ V, the DISP reaction 8 could proceed,[47] causing the second electron transfer to occur by a solution process instead of at an electrode. Two cases of the ECE–DISP mechanism need be considered: ECE–DISP1, reactions 5 + 6 + 8 with reaction 7 negligible; ECE–DISP2, same as DISP1 but with chemical reaction 6 always at equilibrium and forward reaction 8 rate determining. The observed sigmoidal behavior of current function and near-linear variation of $E_{p,c}$ with log v (not shown) are both consistent with an ECE or ECE–DISP mechanism.[46-48] The 27-mV slope of a linear regression plot of $E_{p,c}$ vs. log v marginally favors DISP1 over DISP2.[47c] These two mechanisms are potentially distinguishable because DISP2 is second order.

Table IV. Chronoamperometric Data for $[Fe_2(edt)_4]^{2-}$ in Acetonitrile Solution ([Fe] = 5.3 mM, Glassy-Carbon Electrode, ~25 °C)

t, s	n_{app}/n_1	t, s	n_{app}/n_1	t, s	n_{app}/n_1
0.2	1.19	3.0	1.62	7.0	1.88
0.5	1.38	4.0	1.68	8.0	1.88
1.0	1.50	5.0	1.68	9.0	1.90
2.0	1.50	6.0	1.80	10.0	1.90

Variation of the concentration of $[Fe_2(edt)_4]^{2-}$ to near the solubility limit ([Fe] = 1.4–17 mM) afforded no measurable change in E_p's (±10 mV) at constant scan rate in the 50–500 mV/s range. Although the theoretical concentration dependence $dE_p/d \log C$ = 20 mV at 302 K[47c] is small, the experimental result is best interpreted to indicate the absence of the ECE–DISP2 mechanism.

Any further analysis of the reduction reaction sequence of $[Fe_2(edt)_4]^{2-}$ involves the difficult matter of distinguishing between a pure ECE and an ECE–DISP1 mechanism, the latter being considered a "nuance" of the former.[49] Single- and double-step chronoamperometry[49-51] have been applied to the problem. The

(47) (a) Amatore, C.; Savéant, J. M. *J. Electroanal. Chem. Interfacial Electrochem.* **1978**, *86*, 227; **1980**, *107*, 353. (b) Amatore, C.; Lexa, D.; Savéant, J. M. *Ibid.* **1980**, *111*, 81. (c) Amatore, C.; Gareil, M.; Savéant, J. M. *Ibid.* **1983**, *147*, 1.
(48) Mastragostino, M.; Nadjo, L.; Savéant, J. M. *Electrochim. Acta* **1968**, *13*, 721.
(49) Hawley, M. D.; Feldberg, S. W. *J. Phys. Chem.* **1966**, *70*, 3459.
(50) Murray, R. W. In *Physical Methods of Chemistry. Part IIA. Electrochemical Methods*; Weissberger, A., Rossiter, B. W., Eds.; Wiley-Interscience: New York, 1971; Chapter VIII.

behavior of the function $it^{1/2}$ with time is influenced by the presence of chemical reactions coupled to electrode processes. We consider first the results of single-step measurements, whose current–time dependence is expressed by the Cottrell equation, eq 10.[49] Here A is the electrode area, F is the Faraday, C_{ox} and

$$i_{k=x} = \frac{nFAC_{ox}D_{ox}^{1/2}}{\pi^{1/2}t^{1/2}} \qquad (10)$$

D_{ox} are respectively the bulk concentration and diffusion coefficient of $[Fe_2(edt)_4]^{2-}$, and $k = x$ denotes the kinetic contribution of chemical reaction 6. In the limit of sampling times too short to allow reaction 6 to proceed ($x = 0$) and long enough for it to go to completion ($x = \infty$), $n = n_5$ and $n_5 + n_7$, respectively. At intermediate times the apparent value of n calculated from the Cottrell equation is between n_5 and $n_5 + n_7$ and is given by eq 11.[49] Values of n_{app}/n_5 in Table IV have been calculated from

$$n_{app}/n_5 = it^{1/2}/(it^{1/2})_{k=0} \qquad (11)$$

i–t data collected at sampling times $t = 0.1$–10.0 s, with the denominator of eq 11 taken as 120×10^{-6} A $s^{-1/2}$ evaluated at $t = 0.1$ s.[52] With use of the working curves of n_{app}/n_5 vs. log kt (enlarged from the original) calculated by Hawley and Feldberg,[49] values of kt were obtained for different values of equilibrium constant $K_8 = k_f/k_b$ for reaction 8. Plots of kt vs. t constrained to zero intercept fit best to $K_8 = 1.0$ ($r = 0.9802$), 0/0 ($r = 0.9787$), and 0.1 ($r = 0.9783$) on the basis of the correlation coefficients r.[53] Pseudo-first-order rate constant $k_6 = 0.17$ s^{-1} ($K_8 = 1.0$), 0.21 s^{-1} ($K_8 = 0/0$), and 0.27 s^{-1} ($K_8 = 0.1$) for the three cases. Two of the equilibrium constants require, from eq 12,[49] that the difference in potentials of half-reactions 5 and 7

$$K_8 = \exp\left[-\frac{nF}{RT}(E_7^0 - E_5^0)\right] \qquad (12)$$

is zero. For $K_8 = 0.1$, however, the difference is +60 mV, consistent with an earlier assumption,[45] and $E_5 = -1.13$ V.

In double-step chronoamperometry, the potential step −1.4 to −0.9 V was used and i_a/i_c ratios were determined at $t \leq 0.20$ s. From the working curves of Schwarz and Shain,[51b,54] values of k were obtained, and from these $k_6 = 0.19$ s^{-1}. Considering the errors associated with fast sampling times, this value of the rate constant is in good agreement with that determined by the single-step method. Such criteria as could be applied in the present case for distinguishing ECE and disproportionation mechanisms[47] were not clear-cut. The results of the single-potential-step study marginally favor the ECE–DISP1 over the ECE pathway.

(b) $[Mn_2(edt)_4]^{2-}$. In acetonitrile solution experiments were conducted in the concentration range [Mn] = 8–15 mM where the dimeric form predominates ($N_m = 0.07$–0.13). Coulometric reduction afforded $n = 1.10$ and concomitant bleaching of the original intense green solution. These observations are consistent with the occurrence of overall reaction 13 and/or reaction 14 in Scheme II. The tetrahedral product complex has been isolated and structurally characterized.[1] As in the Fe system, cyclic voltammograms of unreduced and fully reduced solutions are exactly complementary; hence, the reduction reaction(s) is reversible. For reasons unclear, we were able to achieve only n ≅ 0.8 in the coulometric oxidation of $[Mn(edt)_2]^{2-}$ (reverse of reaction 13).

Scheme II

$$[Mn_2(edt)_4]^{2-} + 2e^- \rightleftharpoons 2[Mn(edt)_2]^{2-} \qquad (13)$$

$$[Mn(edt)_2(MeCN)_2]^- + e^- \rightleftharpoons [Mn(edt)_2]^{2-} + 2MeCN \qquad (14)$$

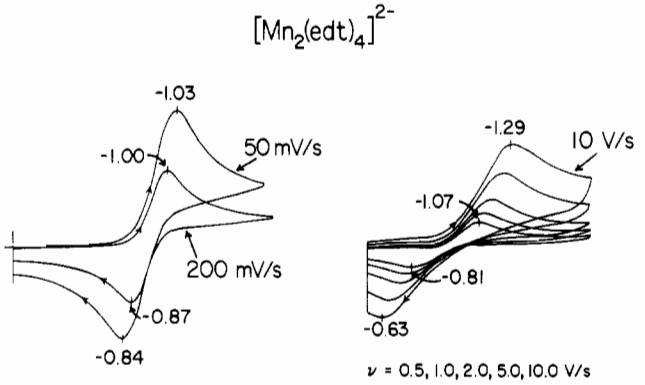

Figure 7. Cyclic voltammograms in the intervals −0.4 to −1.4 V (left) and −1.8 V (right) of an acetonitrile solution of $[Mn_2(edt)_4]^{2-}$ ([Mn] = 14.8 mM) at scan rates of 0.05–10 V/s at a glassy-carbon electrode. Peak potentials are indicated.

Cyclic voltammetry of a solution of $[Mn_2(edt)_4]^{2-}$ in the interval −0.4 to −1.8 V at a glassy-carbon electrode elicited a single redox process. At $v \lesssim 500$ mV/s, $i_{p,a}/i_{p,c} \cong 1$, the cathodic current function is about twice that of $[Mn(edt)_2]^{2-}$, and $E_{1/2} = -0.94$ (1) V. Voltammograms at different scan rates are set out in Figure 7. The potential and current function criteria used in the $[Fe_2(edt)_4]^{2-}$ system point to coupled electron-transfer and chemical reactions. An important difference, however, is that up to a scan rate of 10 V/s, there is no evidence for two cathodic processes at resolvable potentials. It is entirely probable that monomer–dimer equilibrium 1 is very rapidly established and that the potentials of the two species are only slightly different.[45] In this event, only one process would be observed. If events were to follow the sequence of Scheme I, the failure to observe two reductions (with the requisite potential separation) means, in effect, that at 10 V/s it is not possible to outrun the chemical step interposed between electron transfers. Facile dissociation of $[Mn_2(edt)_4]^{2-,3-}$ is expected because of the relatively long Mn–S bridge bond in the dianion (Figure 5) and the same property together with the substitutional lability of Mn(II) in the trianion.

Electrode Effects and Adsorption. The electrochemistry of solutions containing $[M_2(edt)_4]^{2-}$ and $[M(edt)_2(solv)_2]^-$ (M = Fe(III), Mn(III)) was found to be strongly affected by the nature of the electrode and to exhibit characteristics of adsorption. While these effects may be present to varying extents with other complexes, they are by far the most pronounced in the systems described below.

As shown by the voltammograms in Figure 8, the redox behavior of an acetonitrile solution of $[Mn_2(edt)_4]^{2-}$ ($N_m \sim 0.1$) at constant [Mn] and the relatively slow scan rate of 50 mV/s is markedly dependent on the electrode surface. From the ΔE_p values at Pt, glassy carbon (GC), and basal pyrolytic graphite (BPG), the apparent rate of heterogeneous electron transfer follows the order BPG ≳ GC ≫ Pt.[55] The corresponding rate constants k_s at BPG, GC, and Pt electrodes were evaluated by using eq 15,[41,56] in which ψ is a dimensionless rate parameter, α is the

$$k_s = \psi(\pi nFvD_{ox})^{1/2}/(RT)^{1/2}\gamma^{\alpha} \qquad (15)$$

charge-transfer coefficient, $\gamma = (D_{ox}/D_{red})^{1/2}$, D_{ox} and D_{red} are the diffusion coefficients of $[Mn_2(edt)_4]^{2-}$ and $[Mn(edt)_2]^{2-}$, respectively, and the other symbols have their usual meanings. The equality $D_{ox} = D_{red}$ was assumed, and $D_{ox} = 4.6 \times 10^{-6}$ cm^2/s was evaluated from the Randles–Sevčik equation.[57] Using the pre-

(51) (a) Alberts, G. S.; Shain, I. *Anal. Chem.* **1963**, *35*, 1859. (b) Schwarz, W. M.; Shain, I. *J. Phys. Chem.* **1965**, *69*, 30.
(52) That the time interval employed covered the limits of eq 10 is shown by the ratio $(n_5 + n_7)/n_5 = 1.90$ calculated from $it^{1/2}$ values at 0.1 and 10.0 s (Table IV).
(53) Other values include $K_8 = 0$ ($r = 0.9650$), ∞ ($r = 0.9639$), and 10 ($r = 0.9242$), all much less satisfactory than the above.
(54) For an enlarged presentation of working curves, cf.: Geiger, W. E. *Prog. Inorg. Chem.* **1985**, *33*, 275.
(55) Nearly the same order is followed by $[Fe_2(edt)_4]^{2-}$ in acetonitrile but with smaller ΔE_p values, especially at Pt: GC (70) > BPG (90) > Pt (250 mV) ($v = 50$ mV/s).
(56) Nicholson, R. S. *Anal. Chem.* **1965**, *37*, 1351.
(57) Adams, R. N. *Electrochemistry at Solid Electrodes*; Dekker: New York, 1969; pp 124–139. The electrode areas were evaluated by chronoamperometry of a 5 mM $K_4Fe(CN)_6$ solution and use of the diffusion coefficient of $[Fe(CN)_6]^{4-}$ (p 219). As a check, $D_{ox} = 4.8 \times 10^{-6}$ cm^2/s was determined for $[V_2(edt)_4]^{2-}$ in acetonitrile.

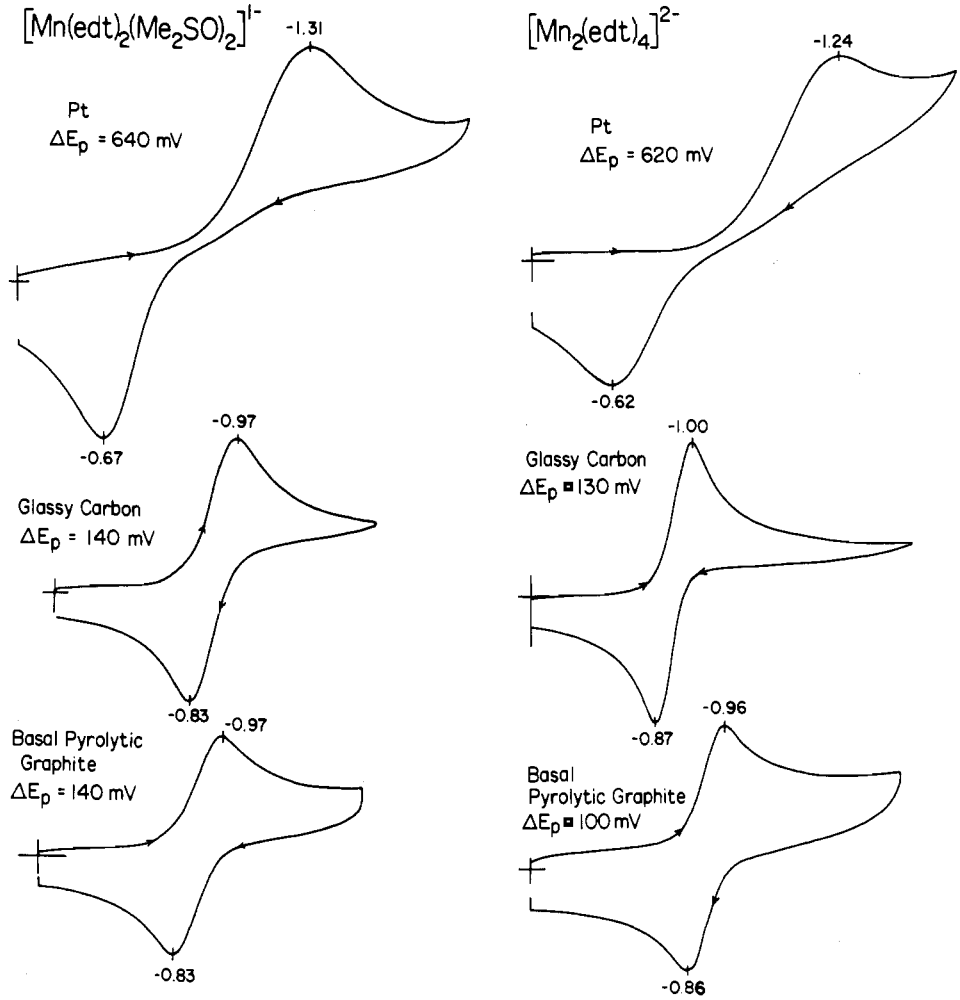

Figure 8. Cyclic voltammograms of $[Mn(edt)_2(Me_2SO)_2]^-$ (7.32 mM) in Me_2SO and $[Mn_2(edt)_4]^{2-}$ ([Mn] = 14.8 mM) in acetonitrile at three different electrodes. All measurements were made at 50 mV/s; peak potential separations are indicated.

dicted variation of $n\Delta E_p$ with log ψ,[56,58] we estimate k_s(app) $\sim 2 \times 10^{-3}$ cm/s (GC), 3×10^{-3} cm/s (BPG), and 4×10^{-6} cm/s (Pt).

In Me_2SO solutions at concentrations where the solvated monomer is present in large excess ($N_m \gtrsim 0.8$), reaction 16 has been demonstrated by coulometry and cyclic voltammetry (Table I). As is evident from Figure 8, the electrode effect on hetero-

$$[Mn(edt)_2(Me_2SO)_2]^- + e^- \rightleftharpoons [Mn(edt)_2]^{2-} + 2Me_2SO \quad (16)$$

geneous electron-transfer rates persists. The values $k_s \sim 1 \times 10^{-3}$ cm/s (GC, BPG) and 3×10^{-6} cm/s (Pt) were obtained as above. (To the extent that IR loss is not fully compensated, these and the preceding k_s values will be larger than the actual rate constants.) In the corresponding Fe system, where the formation of $[Fe(edt)_2]^{2-}$ has been demonstrated, the effect is much smaller. At a GC electrode and $v \leq 200$ mV/s, the reduction reaction is essentially a reversible charge-transfer process.

With differences of $\sim 10^3$ in apparent heterogeneous rate constants (at the fixed scan rate of 50 mV/s), the present systems provide clear examples of electrode dependence of charge-transfer rates. Similar cases, but with a usually much smaller dependence, have been reported recently.[44c,59]

The redox behaviors of $[Fe_2(edt)_4]^{2-}$ and $[Mn_2(edt)_4]^{2-}$ in acetonitrile thus far considered have been based on voltammetry performed in the interval −0.4 to −1.8 V. Differences in behavior are encountered when the initial potential is more anodic, i.e., at or near 0 V. Representative two-scan cyclic voltammograms, recorded at 200 mV/s, are provided in Figure 9. The Fe system displays a sharp spike at −0.95 V in the first scan. By holding the GC electrode at a given potential (−0.3 to +0.2 V) for the fixed time of 20 s, during which time anodic current flows, and then initiating the scan, we established that the amplitude of the −0.95 V feature increased as the initial potential was increased. Further, cyclic voltammetry of a coulometrically generated solution of $[Fe(edt)_2]^{2-}$ displays, in addition to the well-behaved diffusion-controlled couple at $E_{1/2} = -1.13$ V (Figure 6), a broad wave at −0.2 V when the potential excursion is extended to 0 V. In the interval −1.0 to 0 V, only the broad wave and the spike are observed, indicating that they are counterparts. In the initial scan (Figure 9), the spike is due to adsorbed oxidized material, which is partially desorbed at more negative potentials. The shoulder at −1.18 V arises from the diffusion-controlled reduction. The final feature, at $E_{p,c} = -1.58$ V, is assigned as an adsorption postwave[60] from reduction of $[Fe_2(edt)_4]^{2-}$. The reduction product, $[Fe(edt)_2]^{2-}$, desorbs, and reversal of the scan results in oxidation of this species and then the irreversible oxidation at −0.2 V. The electrochemical behavior thereafter is identical with reaction 4 (Figure 6) so long as the anodic potential limit does not exceed −0.4 V. This sort of electrode surface filming and dissolution is observed with, e.g., hydrophobic viologen salts in aqueous solution.[61]

If the GC electrode is initialized at 0 V with the $[Mn_2(edt)_4]^{2-}$ system in acetonitrile and a cathodic scan executed, the only

(58) Perone, S. P. *Anal. Chem.* **1966**, *38*, 1158.
(59) (a) Mukherjee, R. N.; Rajan, O. A.; Chakravorty, A. *Inorg. Chem.* **1982**, *21*, 785. (b) Sharp, P. R.; Bard, A. J. *Inorg. Chem.* **1983**, *22*, 3462. (c) Bond, A. M.; Carr, S. W.; Colton, R. *Organometallics* **1984**, *3*, 541.
(60) Wopschall, R. H.; Shain, I. *Anal. Chem.* **1967**, *39*, 1514.
(61) (a) Jasinski, R. *J. Electrochem. Soc.* **1979**, *126*, 167; **1977**, *124*, 637. (b) Bruinink, J.; Kregting, C. G. A. *Ibid.* **1978**, *125*, 1397. (c) Bruinink, J.; Kregting, C. G. A.; Ponjeé, J. J. *Ibid.* **1977**, *124*, 1854.

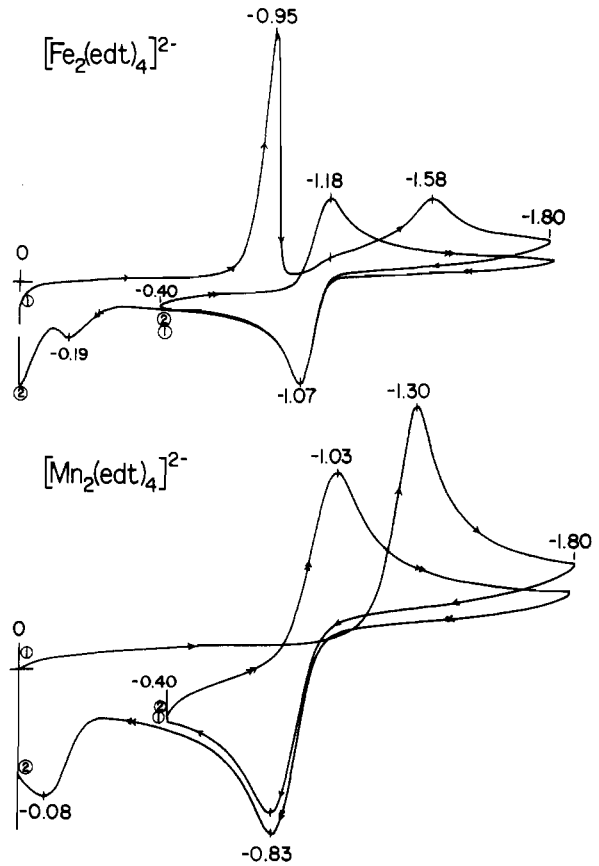

Figure 9. Cyclic voltammograms of $[Fe_2(edt)_4]^{2-}$ ([Fe] = 5.5 mM) and $[Mn_2(edt)_4]^{2-}$ ([Mn] = 9.3 mM) at a glassy-carbon electrode (200 mV/s) in acetonitrile solutions. Initial and terminal points of the first (→) and second (⟶) scans are marked. Peak potentials and scan limits are indicated. Voltammograms were essentially identical at [Fe] = 1.1–5.5 mM and [Mn] = 2.1–17.0 mM.

feature observed to a switching potential of −1.8 V is the relatively sharp aspect with $E_{p,c} = -1.30$ V (Figure 9). Scan reversal results in solution oxidation at −0.83 V and a broad, irreversible oxidation near −0.1 V. If the scan is switched at −0.4 V, only the diffusion-controlled reaction(s) 13/14 (Figure 7) is observed upon further cycling. The feature at −1.30 V is assigned to the reduction of adsorbed $[Mn_2(edt)_4]^{2-}$, the product of which, $[Mn(edt)_2]^{2-}$, is then desorbed. The peak current of this feature is directly proportional to scan rate, indicative of the adsorptive nature of the current.[60] In the anodic portion of the first scan, the anodic trace crosses over the cathodic trace. This type of crossing arises when the product redox couple has a formal potential positive to that of the reactant redox couple.[62] In the present case we postulate that this behavior occurs by means of reaction 17, in which the adsorbed (reactant) couple ($E_{p,c} = -1.30$ V at $v = 200$ mV/s) operates at a more negative potential than does the solution (product) couple ($E_{1/2} = -0.94$ V).

$$[Mn(edt)_2]^{2-}{}_{soln} + [Mn_2(edt)_4]^{2-}{}_{ads} \rightleftharpoons [Mn(edt)_2]^{2-}{}_{ads} + [Mn_2(edt)_4]^{2-}{}_{soln} \quad (17)$$

In both the Fe and Mn systems the adsorption phenomena occur only if the electrode is initialized at potentials more positive than −0.4 V. Acetonitrile solutions of $[Zn(edt)_2]^{2-}$[4] show two irreversible oxidations at $E_{p,a} = -0.40$ and −0.06 V ($v = 200$ mV/s) at a glassy-carbon electrode. Oxidation of coordinated edt is therefore a plausible assignment of the oxidations near 0 V in Figure 9 that cause electrode filming. Clearly the oxidized materials that coat the electrodes in the Fe and Mn systems are largely different, inasmuch as the latter lacks the sharp adsorption spike of the former.

(62) Amatore, C.; Pinson, J.; Savéant, J. M.; Thiebault, A. *J. Electroanal. Chem. Interfacial Electrochem.* **1980**, *107*, 59.

Summary. The following are the principal findings and conclusions of this investigation.

(1) Quaternary cation salts of $[Ti(edt)_3]^{2-}$, $[M(edt)_2]^{2-}$ (M = Cr(II), Co(II)), $[Co(edt)_2]^-$, and $[M_2(edt)_4]^{2-}$ (M = V(III), Mn(III), Fe(III)) are soluble and stable under anaerobic conditions in polar aprotic solvents (MeCN, Me_2SO, DMF), in which they display characteristic absorption spectra dominated by LMCT bands.

(2) All complexes exhibit one chemically reversible redox reaction except for $[Ti(edt)_3]^{2-}$ and $[Cr(edt)_2]^{2-}$, which are irreversibly reduced and oxidized, respectively. Planar $[Co(edt)_2]^-$ and tetrahedral $[Co(edt)_2]^{2-}$ are reversibly interconverted in acetonitrile at $E_{1/2} = -1.16$ V and can be separately generated by controlled-potential electrolysis of solutions prepared from $(Me_4N)_3[Co_2(edt)_4]$, which contains a 1:1 mixture of the two complexes. $[Co(edt)_2]^-$ is one of the few examples of planar, spin-triplet Co(III).

(3) $[V_2(edt)_4]^{2-}$, from its weak paramagnetism, retains its unique tetrabridged structure (**1**) in solution, where it is oxidized to somewhat unstable $[V_2(edt)_4]^-$.

(4) In contrast to $[V_2(edt)_4]^{2-}$, $[M_2(edt)_4]^{2-}$ (M = Mn(III), Fe(III)) complexes show concentration- and solvent-dependent magnetic properties in acetonitrile and Me_2SO that are consistent with the (partial) dissociation of the antiferromagnetic, doubly bridged lateral dimer structure **2** to high-spin solvated monomers. The dimeric form is favored in the weakly coordinating solvent acetonitrile. $[Fe_2(edt)_4]^{2-}$ is not detectably dissociated in this solvent.

(5) Complete reduction of $[M_2(edt)_4]^{2-}$ (reactions 4 and 13) and $[M(edt)_2(solv)_2]^-$ (reactions 7, 14, and 16) (M = Mn(III), Fe(III)) results in formation of tetrahedral $[M(edt)_2]^{2-}$; $[Mn(edt)_2]^{2-}$ has been previously isolated.[1] This is one of the few instances of dimer $\xrightarrow{2e^-}$ monomer electrochemical cleavage of a metal complex,[35,36,63] the most familiar prior cases being the reductions $[M_2(S_2C_2R_2)_4]^{2-} \rightarrow 2[M(S_2C_2R_2)_2]^{2-}$ of M = Fe and Co dithiolenes.[35,36,63b] Unlike the latter, whose nonclassical delocalized electronic structures stabilize the more highly oxidized dimers $[M_2(S_2C_2R_2)_4]^{-,0}$, such species are not attainable with the classical edt complexes.

(6) At fast scan rates in cyclic voltammetry the three-membered electron-transfer series (9) is detectable. The ECE–DISP1 mechanism is marginally favored over the ECE mechanism for the reduction of $[Fe_2(edt)_4]^{2-}$ in acetonitrile in overall reaction 4.[64] Single-and double-potential-step chronoamperometry afforded $k \approx 0.2$ s^{-1} for the chemical step of $[Fe_2(edt)_4]^{3-}$ dissociation (reaction 6) separating the two electron-transfer processes. Resolvable one-electron reductions of the $[Mn_2(edt)_4]^{2-}$ system in acetonitrile were not observed, apparently due to rapid monomer–dimer equilibration promoted by relatively weak Mn–S bridge bonds.

(7) The voltammetry of $[Mn_2(edt)_4]^{2-}$ and $[Mn(edt)_2(solv)_2]^-$ (solv = MeCN, Me_2SO) is markedly electrode-dependent, with heterogeneous electron-transfer rate constants $\sim 10^3$ larger at clean GC and BPG electrodes than at a clean Pt electrode. $[Fe_2(edt)_4]^{2-}$ and $[Mn_2(edt)_4]^{2-}$ systems in acetonitrile exhibit definite adsorption behavior on a clean GC electrode when cathodic scans are initiated at or near 0 V. These systems are free of adsorption artifacts when the rest potential is properly taken as ca. −0.4 V.

The results of (7) lead to clarification of some unusual results reported earlier. Very large peak potential differences in the 0.5–0.8-V range have been reported for DMF and acetonitrile solutions prepared from $[Mn_2(edt)_4]^{2-}$.[1,6] In one case,[6] a switching potential of −0.1 V was used (v unspecified), sufficient to cause electrode filming and a behavior similar to that in Figure 9. The

(63) (a) $M_2(CO)_{10} \rightarrow 2[M(CO)_5]^-$ (M = Mn, Re): ref 44a and references therein. (b) $[Co_2(mnt)_4]^{2-} \rightarrow 2[Co(mnt)_2]^{2-}$: Vlček, A., Jr.; Vlček, A. A. *J. Electroanal. Chem. Interfacial Electrochem.* **1981**, *125*, 481.

(64) For recent reports describing differentiation of the two mechanisms in favor of ECE, cf. ref 47ab and the following: (a) Lexa, D.; Savéant, J. M.; Zickler, J. *J. Am. Chem. Soc.* **1980**, *102*, 2654. (b) Marrese, C. A.; Carrano, C. J. *Inorg. Chem.* **1984**, *23*, 3961. (c) Al-Salih, T. I.; Pickett, C. J. *J. Chem. Soc., Dalton Trans.* **1985**, 1255.

even larger ΔE_p = 1.15 V for $[Mn(edt)_2(HIm)]^-$[12] (v and scan limits unspecified) presumably arises in the same way. $[Mn(tdt)_2]^-$ is reported to be reduced at $E_{p,c}$ = −1.09 V with ΔE_p = 0.61 V in a DMF solution at a Pt electrode (v = 100 mV/s).[11] We have reproduced this result and also have shown that at a GC electrode ΔE_p is diminished to 0.11 V (Table I). This behavior closely resembles that in Figure 8 and is ascribed to significantly different k_s values at the two electrode surfaces. While the reduction/oxidation cycle of $[Mn(edt)_2(solv)_2]^-$ (reactions 14 and 16) must involve the structural and spin changes previously described,[1] it is now evident that the large ΔE_p values observed in Mn–edt and Mn–tdt systems do not demonstrably derive from them. Instead, any such kinetics effects arising in this way that would cause deviations from reversible charge transfer are overridden by slow heterogeneous electron transfer and adsorption. This is made particularly evident by reaction 18 in acetonitrile, which carries

$$[Co(edt)_2]^- \text{ (planar, } S = 1) + e^- \underset{}{\overset{-1.16\text{ V}}{\rightleftharpoons}} [Co(edt)_2]^{2-} \text{ (tetrahedral, } S = {}^3/_2) \quad (18)$$

a structural and a spin change (involving σ^* orbitals). Under the same conditions where the Mn systems exhibit large ΔE_p values, this reaction is one of reversible charge transfer (Table I). As in at least one prior case,[59b] examination of redox reactions at more than one electrode surface has shown that interpretation of large ΔE_p values solely in terms of structural changes accompanying charge transfer is incorrect. The electrochemistry associated with numerous processes of this type has been characterized.[54,65]

Acknowledgment. This research was supported by NIH Grant GM-28856. We thank Professors F. C. Anson and M. S. Wrighton for useful discussions and Professor Anson for several preliminary electrochemical measurements.

Registry No. 2 (M = Mn^{III}), 87526-32-7; **2** (M = Fe^{III}), 46847-88-5; $[Ti(edt)_3]^{2-}$, 94750-77-3; $[V_2(edt)_4]^{2-}$, 87145-61-7; $[Cr(edt)_2]^{2-}$, 94750-79-5; $[Mn(edt)_2]^{2-}$, 87526-34-9; $[Fe(edt)_2]^{2-}$, 102920-35-4; $[Co(edt)_2]^-$, 94750-83-1; $[Co(edt)_2]^{2-}$, 94750-82-0; $[Mn(tdt)_2]^{2-}$, 94595-52-5; $[Mn(tdt)_2]^-$, 94500-28-4; $[Fe(tdt)_2]^-$, 14874-42-1; $[Co(tdt)_2]^-$, 52152-14-4; $[Mn(edt)_2(Me_2SO)]^-$, 102920-36-5; $[Mn(edt)_2(Me_2CN)_2]^-$, 87802-61-7; $[Fe(edt)_2(Me_2CN)_2]^-$, 102920-37-6; Pt, 7440-06-4; carbon, 7440-44-0; graphite, 7782-42-5.

(65) Gaudiello, J. G.; Wright, T. C.; Jones, R. H.; Bard, A. J. *J. Am. Chem. Soc.* **1985**, *107*, 888 and references therein.

Contribution from the Department of Chemistry, University of Florida, Gainesville, Florida 32611

Solution Chemistry of Rhodium Trifluoroacetate in the Presence of Phosphorus Donors

Joshua Telser and Russell S. Drago*

Received November 2, 1984

$^{31}P\{^1H\}$ and ^{19}F NMR studies on $Rh_2(O_2CCF_3)_4(PY_3)_2$ where Y = OPh, Ph, or Cy (cyclohexyl) are described. The $^{31}P\{^1H\}$ NMR spectrum of the $P(OPh)_3$ adduct shows an AA′XX′ (A, A′ = ^{103}Rh; X, X′ = ^{31}P) system, as expected for an axial (class I) adduct. A single ^{19}F signal is observed. A similar spectrum is also seen for $Rh_2(O_2CCH_2CH_2CH_3)_4(PPh_3)_2$. The $^{31}P\{^1H\}$ NMR spectra of the PPh_3 and PCy_3 adducts both show three signals due to the presence in solution of an axial (class I) and axial/equatorial (class III) phospine coordinated Rh dimer. This solution behavior is in contrast to their class I solid-state structure. $Rh_2(O_2CCF_3)_4$ reacts with excess PCy_3 to give monomeric Rh(I) and Rh(III) species. The $^{31}P\{^1H\}$ and ^{19}F NMR spectra of $Rh(O_2CCF_3)_2(P(OMe)_3)_3$ are reported and support the true formulation of the complex as $Rh(P(OMe)_3)_4^+Rh(O_2CCF_3)_4(P(OMe)_3)_2^-$. A mechanism is proposed for cleavage of the Rh^{II}_2 complex to Rh(I) and Rh(III) monomers involving ligand-induced polarization of the Rh–Rh bond.

Introduction

Complexes of general formula $Rh_2(O_2CR)_4L_2$ have been widely studied in the solid state,[1] and all have axially coordinated Lewis bases. This structural type has been called class I by Andersen.[2] With $Mo_2(O_2CCF_3)_4$, Lewis base coordination equatorial to the Mo–Mo bond has been reported in the solid state[2,3] and in solution[4] to give what are referred to as class II complexes.[2] In a previous study from this laboratory,[5] we found that both axial and equatorial ligand coordination occurred to one dimeric $Rh_2(O_2CCF_3)_4$ unit in the presence of excess pyridine and *tert*-butyl isocyanide, which we call class III behavior. Furthermore, it was found that with phosphorus donors unusual solution behavior was observed even without excess ligand. In the presence of excess ligand, Rh–Rh bond cleavage occurred much more readily with phosphorus than with other donors. We have extended and clarified these earlier studies and find definitive evidence for the unusual behavior of $Rh_2(O_2CCF_3)_4$ in the presence of phosphorus donor bases.

Results and Discussion

The previously reported[5] ^{19}F NMR spectrum of $Rh_2(O_2CCF_3)_4(P(OPh)_3)_2$ (before decomposition occurred) showed a single peak corresponding to the four equivalent $CF_3CO_2^-$ ligands, suggestng a class I (axial) structure in solution.

The $^{31}P\{^1H\}$ NMR spectrum of $Rh_2(O_2CCF_3)_4(P(OPh)_3)_2$ obtained earlier in $CDCl_3$ at room temperature on a 100-MHz instrument provided inconclusive structural information since extensive ligand oxidation occurred to form $OP(OPh)_3$.[5] In the present study a 300-MHz ^1H (121.5 MHz for ^{31}P) instrument was used, which gave better resolution, required less data aquisition time, and required less sample. Furthermore, the $CDCl_3$ solution of $Rh_2(O_2CCF_3)_4(P(OPh)_3)_2$ was frozen at −70 °C immediately after prepartion to inhibit the phosphite oxidation process. The $^{31}P\{^1H\}$ NMR spectrum of $Rh_2(O_2CCF_3)_4(P(OPh)_3)_2$ obtained in this manner showed no signal attributable to phosphate. The $^{31}P\{^1H\}$ NMR signal obtained here showed a quartet, but with the center peaks very close at −50 °C. $Rh_2(O_2CCF_3)_4(P(OPh)_3)_2$ is an AA′XX′ spin system (A, A′ = ^{103}Rh; X, X′ = ^{31}P). The outer lines are separated by $|J_{AX} + J_{AX'}| = |^1J_{Rh-P} + {}^2J_{Rh-P}| =$ 134.5 Hz. All ^{31}P NMR data are summarized in Table I. The separation of the inner lines (11.5 Hz at −150 °C) is either $[((J_{AA'}$

(1) Cotton, F. A.; Walton, R. A. *Multiple Bonds Between Metal Atoms*; Wiley-Interscience: New York, 1982. Felthouse, T. R. *Prog. Inorg. Chem.* **1982**, *29*, 73.
(2) Girolami, G. S.; Mainz, V. V.; Andersen, R. A. *Inorg. Chem.* **1980**, *19*, 805.
(3) Cotton, F.A.; Lay, D. G. *Inorg. Chem.* **1981**, *20*, 935.
(4) Webb, T. A.; Dong, T. Y. *Inorg. Chem.* **1982**, *21*, 935.
(5) Telser, J.; Drago, R. S. *Inorg. Chem.* **1984**, *23*, 2599.

0020-1669/86/1325-2989$01.50/0